The FEBS Journal

FEBS PRESS science publishing by scientists

Increased demand for FAD synthesis in differentiated and stem pancreatic cancer cells is accomplished by modulating *FLAD1* gene expression: the inhibitory effect of Chicago Sky Blue

Alessia Nisco[1], Tiago M. A. Carvalho[1], Maria Tolomeo[1,2], Daria Di Molfetta[1], Piero Leone[1], Michele Galluccio[2], Milagros Medina[3], Cesare Indiveri[2,4], Stephan Joel Reshkin[1], Rosa Angela Cardone[1] and Maria Barile[1]

1 Department of Biosciences, Biotechnologies, and Environment, University of Bari Aldo Moro, Italy
2 Department of DiBEST (Biologia, Ecologia e Scienze della Terra), University of Calabria, Arcavacata di Rende, Italy
3 Departamento de Bioquímica y Biología Molecular y Celular, Facultad de Ciencias, Instituto de Biocomputación y Física de Sistemas Complejos (BIFI) (GBsC-CSIC Joint Unit), University of Zaragoza, Spain
4 CNR Institute of Biomembranes, Bioenergetics and Molecular Biotechnologies (IBIOM), Bari, Italy

Keywords
cancer stem cells; Chicago Sky Blue; *FLAD1*; flavoenzymes; PDAC

Correspondence
M. Barile, Department of Biosciences, Biotechnologies, and Environment, University of Bari Aldo Moro, Via Orabona 4, 70125 Bari, Italy
Tel: +390805443604
E-mail: maria.barile@uniba.it

(Received 13 January 2023, revised 31 March 2023, accepted 30 May 2023)

doi:10.1111/febs.16881

FLAD1, along with its FAD synthase (FADS, EC 2.7.7.2) product, is crucial for flavin homeostasis and, due to its role in the mitochondrial respiratory chain and nuclear epigenetics, is closely related to cellular metabolism. Therefore, it is not surprising that it could be correlated with cancer. To our knowledge, no previous study has investigated *FLAD1* prognostic significance in pancreatic ductal adenocarcinoma (PDAC). Thus, in the present work, the FAD synthesis process was evaluated in two PDAC cell lines: (a) PANC-1- and PANC-1-derived cancer stem cells (CSCs), presenting the R273H mutation in the oncosuppressor p53, and (b) MiaPaca2 and MiaPaca2-derived CSCs, presenting the R248W mutation in p53. As a control, HPDE cells expressing wt-p53 were used. FADS expression/activity increase was found with malignancy and even more with stemness. An increased FAD synthesis rate in cancer cell lines is presumably demanded by the increase in the FAD-dependent lysine demethylase 1 protein amount as well as by the increased expression levels of the flavoprotein subunit of complex II of the mitochondrial respiratory chain, namely succinate dehydrogenase. With the aim of proposing FADS as a novel target for cancer therapy, the inhibitory effect of Chicago Sky Blue on FADS enzymatic activity was tested on the recombinant 6His-hFADS2 (IC_{50} = 1.2 μM) and PANC-1-derived CSCs' lysate (IC_{50} = 2–10 μM). This molecule was found effective in inhibiting the growth of PANC-1 and even more of its derived CSC line, thus assessing its role as a potential chemotherapeutic drug.

Abbreviations
CSB, Chicago Sky Blue; CSC, cancer stem cell; FAD, flavin adenin dinucleotide; FADS, FAD synthase; FMN, flavin mononucleotide; GAPDH, glyceraldehyde-3-phosphate dehydrogenase; GOF, gain of function; Gos, gossypol; HPDE, human pancreatic ductal epithelioid; LSD1, lysine demethylase 1; PAPS, 3′-phosphoadenosine 5′-phosphosulfate; PDAC, pancreatic ductal adenocarcinoma; Rf, riboflavin; RT-PCR, reverse transcriptase polymerase chain reaction; SDHA, succinate dehydrogenase subunit A.

Introduction

Pancreatic ductal adenocarcinoma (PDAC) is one of the most lethal human malignancies and the fourth leading cause of cancer-related deaths. Even though there have been significant efforts to enhance clinical results, PDAC resistance to conventional chemotherapeutics remains a clinical problem [1]. Cancer stem cells (CSCs) are a small subset of cells that are distinguished by their ability to self-renew, distinct metabolism and resistance to anticancer agents [2]. In several tumours, including PDAC, CSCs have been identified as drivers of tumour initiation and progression as well as the primary cause of resistance to standard chemotherapeutics [3]. Notably, CSCs' distinct plasticity makes them especially well-suited to adaptation to metabolic or oxidative stress [4]. CSCs generally have an increased mitochondrial mass and a higher dependence on mitochondrial biogenesis and oxidative phosphorylation (OXPHOS) for their successful propagation [2].

Flavin adenine dinucleotide (FAD) is an important cofactor for several client flavoenzymes, that is, lysine demethylase 1 (LSD1), flavoprotein subunit of succinate dehydrogenase (SDHA), mainly located in mitochondria. FAD conversion from riboflavin (Rf) requires the consequential actions of riboflavin kinase (RFK, EC2.7.1.26) encoded by *RFK* and FAD synthase or FMN:ATP adenylyl transferase (FADS, EC2.7.7.2) encoded by *FLAD1*. This latter gene, located on chromosome 1 at 1q21.3, codes for different-sized polypeptides, corresponding to different transcript variants generated by alternative splicing of the gene [5,6]. Subsequently, a nuclear localization for FADS was proven to be correlated with the biogenesis of nuclear flavoproteins [7,8]. When the human gene was initially identified by our group, two protein isoforms were described: hFADS1 in the mitochondria [9] and hFADS2 in the cytosol [6,10]. An interesting feature of both characterized FADSs is that they are organized into two domains, the N-terminal resembling molybdopterin-binding domain (MPTb) [11], fused with the C-terminal 3′-phosphoadenosine 5′-phosphosulfate (PAPS) reductase domain, which was recently renamed FADSy since it is able *per se* to perform the FADS activity [12]. In 2016, the shortest isoform (isoform 6), containing the sole PAPS domain, was discovered by Olsen and colleagues [6] and characterized so far by our group [13].

The association between Rf transport and cancer has been addressed in the past [14]. Starting from the identification of the three Rf transporters 1-3 (RFVT1-3), the alteration of their expression in different types of cancer was investigated, including gastric [15], glioma [16], oesophageal [17], cervical [18], breast [19] and colorectal [20]. All these data led us to affirm that cancer cells become greedy for the vitamin. Only a small number of studies have found a link between *FLAD1* expression changes and tumour progression: in 2020, it was found that *FLAD1* is a valuable biomarker for the prognosis of gastric cancer [21]. Furthermore, a search of the Oncomine database (https://www.oncomine.com/) revealed that *FLAD1* overexpression is correlated with a poor prognosis for breast cancer [22].

To date, very little is known about the relationship between *FLAD1* and PDAC. To fill this gap, we analysed the process of FAD synthesis in the highly malignant PDAC cell line PANC-1, which has the gain-of-function (GOF) R273H mutation in the oncogene p53 [23] and in its derived CSCs. Further analyses were also performed on the malignant MiaPaCa2 PDAC cell line, having the GOF R248W mutation [23], and its derived CSCs. As a control, we used human pancreatic ductal epithelioid (HPDE) cells expressing wtp53, which are immortalized but not fully transformed [24].

Furthermore, the effect of the small molecule inhibitor Chicago Sky Blue (CSB) [25] on FADS enzymatic activity was also tested in these cells, with the aim to specifically target the increased flavin metabolism of the CSCs and propose FADS as a novel therapeutic target for PDAC.

Results

The expression levels of FADS and certain flavoenzymes increase in CSCs

First, we investigated FADS protein expression levels with immunoblotting analysis as described in Materials and methods, in HPDE and the highly malignant PDAC cell line PANC-1, carrying the R273H mutation in p53 and its derived CSCs generated as reported [26,27]. Faint bands migrating at different molecular weights were revealed in HPDE. In PANC-1 and PANC-1-derived CSCs, we observed a main band that migrates at about 54 kDa, corresponding to the cytosolic hFADS2 and a minor band migrating at about 42 kDa, which presumably corresponds to a still uncharacterized isoform. The 54 kDa isoform is significantly increased in both PANC-1 (2.8-fold, $*p < 0.05$) and PANC-1-derived CSCs (6-fold, $**p < 0.01$) compared to HPDE (Fig. 1A). Conversely, the lower migrating band does not significantly change in any of the lysates tested. To investigate if the increased FADS

protein content in PANC-1 cells and their derived CSCs is due to transcriptional control, *FLAD1* transcript levels were evaluated by RT-PCR analysis, showing they were in line with the results obtained with immunoblotting (Fig. 1B).

Since the role of FADS is to provide the cofactor to a number of client flavoproteins mainly localized in mitochondria, we first evaluated the protein levels of SDHA, which transfers reducing equivalents from succinate to ubiquinone (coenzyme Q) and is crucial for oxidative metabolism [28]. SDHA, similarly to succinate dehydrogenase subunit B (SDHB) [29], is expected to be modulated in stemness. Indeed, immunoblotting analysis revealed an approximate two-fold increase ($*p < 0.05$) in SDHA protein levels in PANC-1-derived CSCs compared to both HPDE and PANC-1 (Fig. 2A). SDHA flavinylation level (FAD covalently bound per monomer of protein), assayed by on-gel UV fluorescence as described in [30–32], paralleled the protein amount (Fig. 2A, inset), thus proving that there is an increase in the levels of the protein conjugated to FAD, suggesting that the cofactor is not limiting. The analysis of *SDHA* transcript levels also revealed a significant increase in PANC-1-derived CSCs with respect to HPDE and PANC-1 (Fig. 2B).

Another flavoenzyme that is expected to be relevant in tumour transformation is LSD1 [33], a FAD-dependent amine oxidase (AO) that catalyses the demethylation of mono- and dimethyl groups on H3K4 and H3K9, triggering transcriptional repression and activation respectively [34]. We have found that LSD1 obtains its cofactor FAD via the physical interaction with FADS [8,35]. Immunoblotting analysis revealed a significant increase in LSD1 expression with tumorigenicity and stemness (Fig. 2C), and this is substantially in line with the observed increase in the transcript levels (Fig. 2D).

Thus, in p53-mutated cells (PANC-1 and PANC-1-derived CSCs), the increase in expression of relevant flavoenzymes seems to be coordinated with an increase in the efficacy of FAD formation machinery.

To further substantiate this hypothesis, we performed immunoblotting experiments on a PDAC cell line carrying another p53 mutation (R248W), that is, MiaPaCa-2 and its derived CSCs, and essentially the same profile of increment in protein levels of FADS, SDHA and LSD1 was observed (Figs 3 and 4A,B).

We conclude that the observed significant increase in FADS results from oncogenic processes; maybe it is necessary to not limit client flavoenzyme biogenesis in malignant conditions [2]. Consistently, a search in the cBioPortal for Cancer Genomics database (www.cbioportal.org) revealed that *FLAD1* is highly amplified in the pancreatic cancer, with the highest incidence (23.8%) among different tumour types (Fig. 5A). Furthermore, clinical data showed an association between *FLAD1* amplification and reduced patient survival (Fig. 5B).

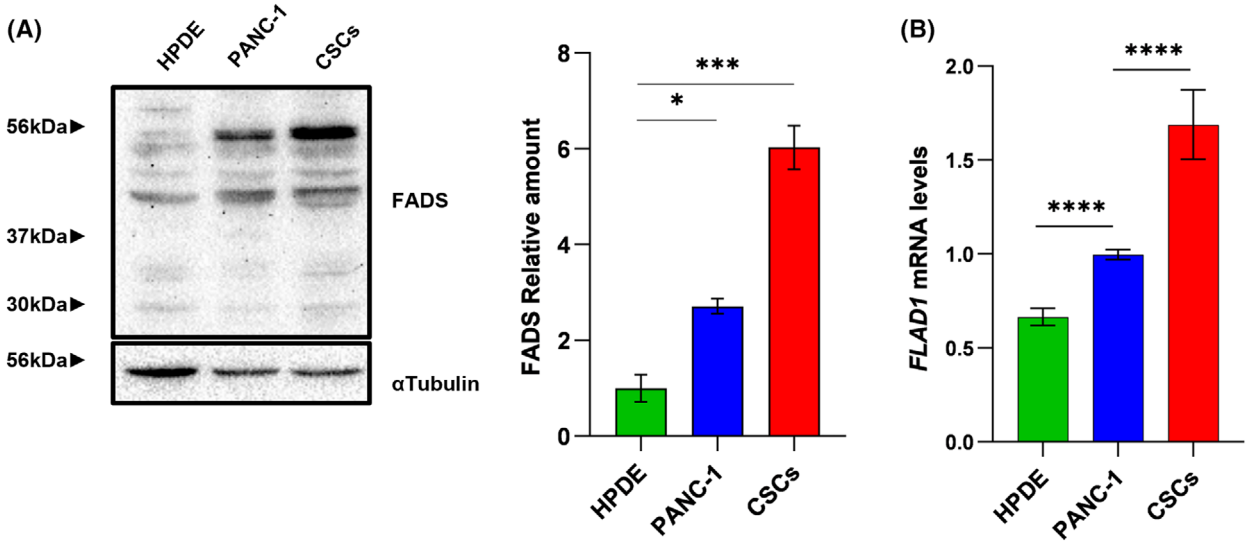

Fig. 1. FADS expression levels in HPDE-, PANC-1 and PANC-1-derived CSCs. (A) HPDE-, PANC-1 and PANC-1-derived CSCs cell lysates were separated by SDS/PAGE and immunoblotted with anti-FADS antibody. 54 kDa protein band intensities were normalized to that of α-tubulin and data were reported as relative quantity with respect to HPDE. All data represent the results of at least three different experiments (mean ± SEM). (B) *FLAD1* mRNA levels in HPDE-, PANC-1 and PANC-1-derived CSCs. Data were normalized to the housekeeping gene *ACTB (β-actin)* and reported as relative quantity with respect to PANC-1. All data represent the results of three different experiments (mean ± SEM). Student's t-test: $*p \leq 0.05$, $***p \leq 0.001$ and $****p \leq 0.0001$.

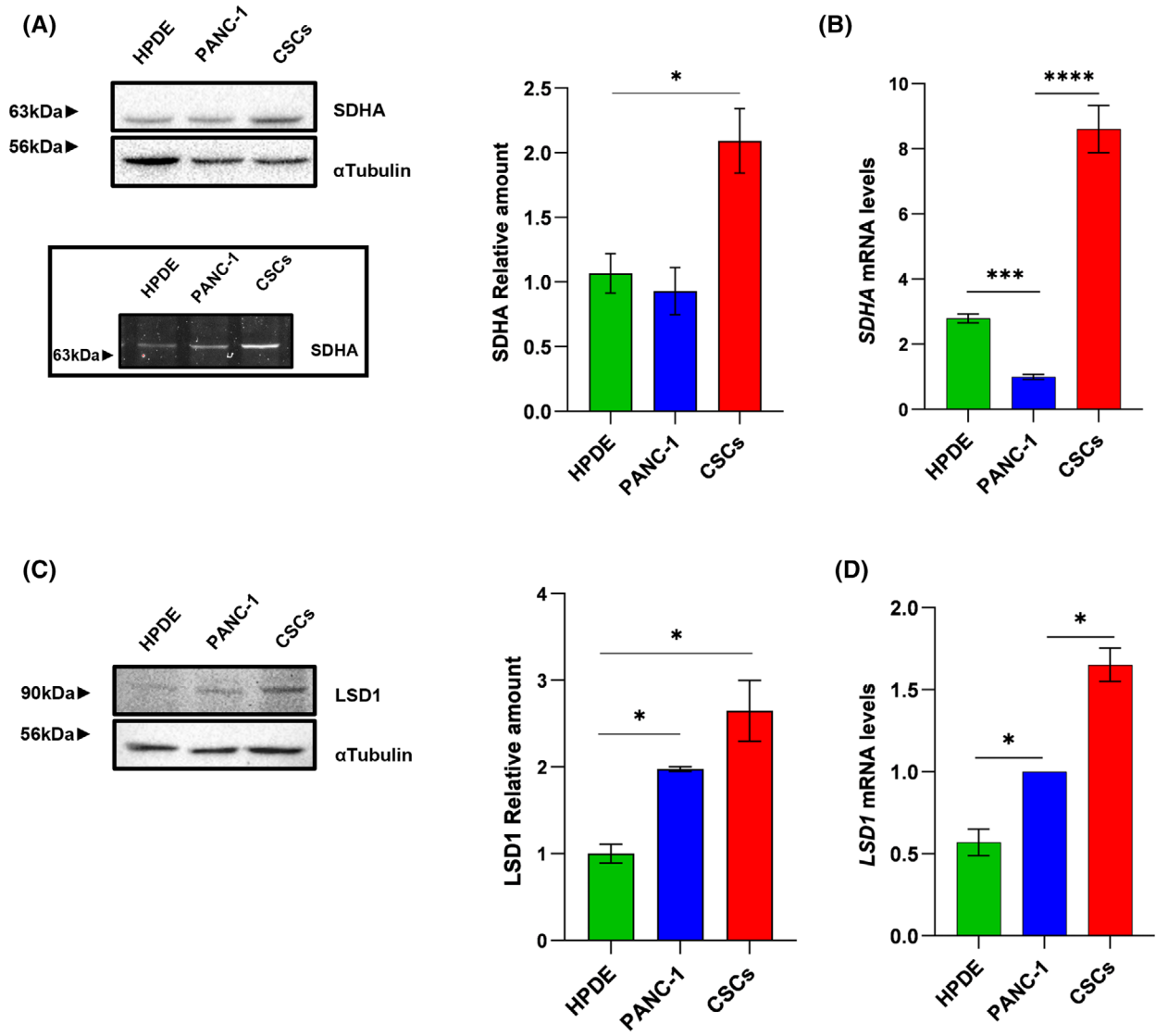

Fig. 2. SDHA and LSD1 expression levels in HPDE-, PANC-1 and PANC-1-derived CSCs. (A) HPDE-, PANC-1 and PANC-1-derived CSCs cell lysates were separated by SDS/PAGE and immunoblotted with a monoclonal anti-SDHA antibody. Protein band intensities were normalized to that of α-tubulin and data were reported as relative quantity with respect to HPDE. All data for SDHA represent the results of at least four different experiments (mean ± SEM). In the inset SDHA flavinylation level, 40 μg of HPDE-, PANC-1 and PANC-1-derived CSCs protein were separated by SDS/PAGE. The flavin fluorescence of SDHA protein was visualized by UV irradiation of the unstained gel soaked in 10% acetic acid. Quantitative evaluation of fluorescence and protein amount was carried out using the Chemidoc Imaging System. (B) *SDHA* mRNA levels in HPDE-, PANC-1 and PANC-1-derived CSCs. Data were normalized to the housekeeping gene ACTB (*β-actin*) and reported as relative quantity with respect to PANC-1. All data represent the results of two different experiments (mean ± SEM). (C) HPDE-, PANC-1 and PANC-1-derived CSCs cell lysates were separated by SDS/PAGE and immunoblotted with anti-LSD1 antibody. Protein band intensities were normalized to that of α-tubulin and data were reported as relative quantity with respect to HPDE. All data for LSD1 represent the results of two different experiments (mean ± SEM). (D) *LSD1* mRNA levels in HPDE-, PANC-1 and PANC-1-derived CSCs. Data were normalized to the housekeeping gene *ACTB* (*β-actin*) and reported as relative quantity with respect to PANC-1. All data represent the results of two different experiments (mean ± SEM). Student's t-test: $*p \leq 0.05$, $***p \leq 0.001$ and $****p \leq 0.0001$.

FAD synthesis rate is faster in PDAC cell lines compared to HPDE

Given the increased expression levels of FADS in malignant cells compared to HPDE, we evaluated whether the increase in protein expression corresponds to a faster synthesis of FAD. To this aim, the time course of FAD synthesis was followed by high-performance liquid chromatography (HPLC) catalysed by

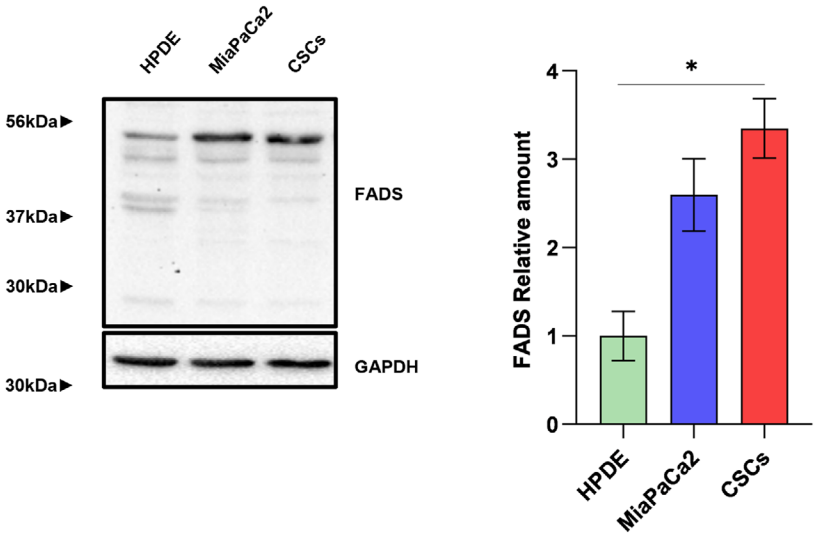

Fig. 3. Immunoblotting analysis of FADS protein in HPDE, MiaPaCa2 and MiaPaCa2-derived CSCs. HPDE, MiaPaCa2 and MiaPaCa2-derived CSCs cell lysates were separated by SDS/PAGE and immunoblotted with anti-FADS antibody. 54 kDa protein band intensities were normalized to that of GAPDH and data were reported as relative quantity with respect to HPDE. All data represent the results of at least two different experiments (mean ± SEM). Student's t-test: *$p \leq 0.05$.

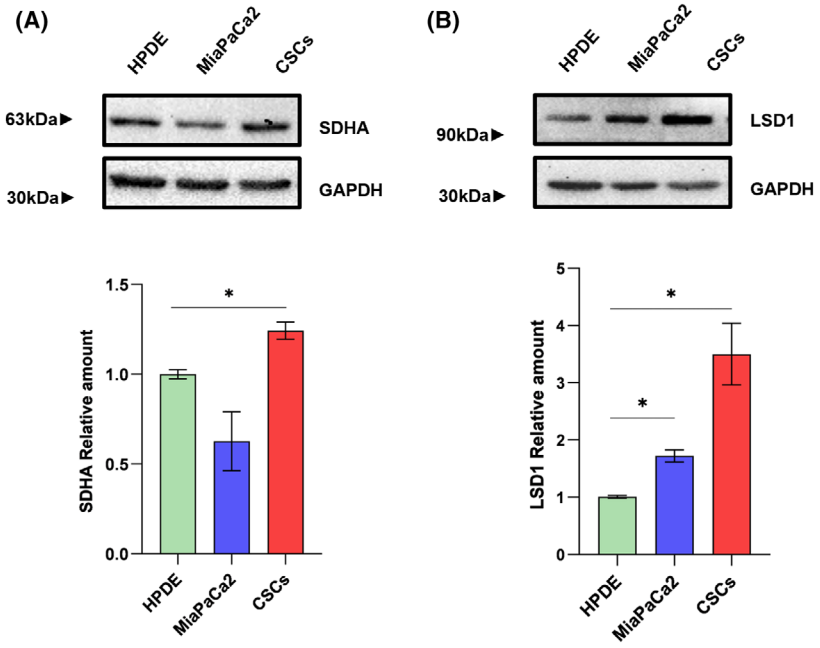

Fig. 4. Immunoblotting analysis of SDHA and LSD1 proteins in HPDE, MiaPaCa2 and MiaPaCa2-derived CSCs. HPDE, MiaPaCa-2 and MiaPaCa2-derived CSCs cell lysates were separated by SDS/PAGE and immunoblotted with (A) anti-SDHA and (B) anti-LSD1 antibodies. Protein band intensities were normalized to that of GAPDH and data were reported as relative quantity with respect to HPDE. All data represent the results of at least two different experiments (mean ± SEM). Student's t-test: *$p \leq 0.05$.

cell lysates, in the presence of FMN 1 μM, ATP 5 mM and $MgCl_2$ 5 mM, as previously described [36].

Figure 6A shows a typical experiment obtained with lysates from PANC-1-derived CSCs. A rapid decrease in FMN occurred due to its enzymatic conversion into its products, that is, FAD and Rf. FAD appearance increased linearly for the first 10 min and reached a plateau within 30 min. Concomitantly with FAD synthesis, the appearance of Rf from FMN was observed, presumably due to unspecific alkaline phosphatases (ALP) present in the cell lysates [37]. FMN hydrolysis to Rf proceeded at an initial rate of 37.0 pmol·mg^{-1}·min^{-1}, therefore disturbing, with increasing incubation time intervals, the process of FAD formation from FMN.

Moreover, to be sure that the reaction of FAD appearance was specifically catalysed by FADS, parallel experiments were performed either in the absence of $MgCl_2$, which is an essential cofactor for FADS-mediated reaction, or in the presence of $HgCl_2$ (Fig. 6B), a known inhibitor of the enzyme [13].

The initial FAD synthesis rate was then evaluated in PANC-1 and HPDE cell lysates. In agreement with the immunoblotting assays (Fig. 1A), the FAD synthesis rate is much higher in PANC-1 CSCs (19.4 pmol·mg^{-1}·min^{-1}) compared to both PANC-1 (4.8 pmol·mg^{-1}·min^{-1}) and

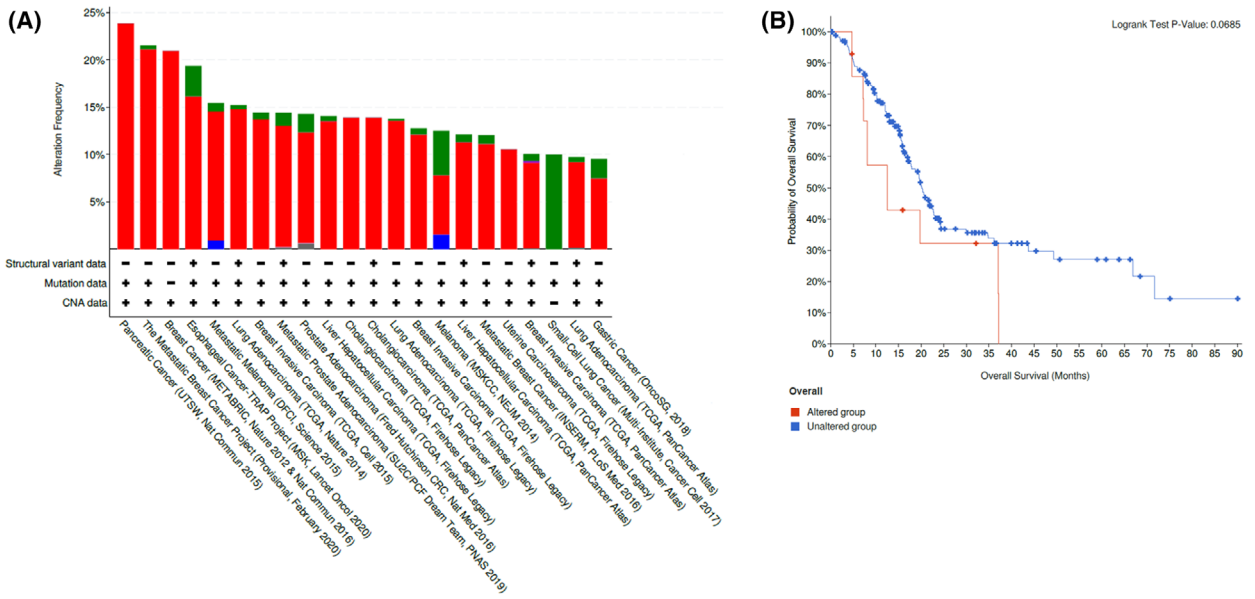

Fig. 5. *FLAD1* genetic alterations reduce survival of pancreatic cancer patients. (A) Representation of *FLAD1* genetic alterations across different cancers (www.cbioportal.org). In red «Amplification», grey «Multiple alterations», green «Mutation» and blue «Deep deletion». (B) Median overall survival data of pancreatic carcinoma patients with *FLAD1* amplification and no amplification.

HPDE (0.2 pmol·mg^{-1}·min^{-1}) (Fig. 6C). We conclude that the CSCs are greedy for flavin cofactors and this could be linked to the observed increase in FAD demand by nascent client flavoenzymes. This scenario makes FADS a potential novel target for cancer therapy.

FAD synthesis rate performed by both recombinant hFADS2 and cell lysates is inhibited by the presence of CSB

Based on the proposal that FADS might be a novel target for cancer therapy, we searched for specific inhibitors for this enzyme. Kinetic experiments were performed on the recombinant 6-His hFADS2 protein, isolated from *E. coli* transformed with the plasmid pH6EX3. This enzyme has been characterized in detail both kinetically and molecularly in our laboratories [38].

In order to find potential FADS inhibitors, we looked to a study [39], in which a series of compounds with antimicrobial activity were identified for targeting the FADS of *Corynebacterium ammoniagenes* (*Ca*FADS). The IC_{50} (half-maximum inhibitory concentration) and the residual activity of *Ca*FADS were examined to assess the efficacy of these compounds. The best-performing compounds for prokaryotic FADS were found to be gossypol (Gos), flunixin meglumine and CSB, whose structures are shown in Fig. 7.

We measured the activity of FADS in the presence of increasing concentrations of each compound. We carried out two sets of experiments with two distinct substrates' concentrations: (i) 0.3 μM FMN, 25 μM ATP and (ii) 2 μM FMN, 100 μM ATP. In the first condition (i), with 50 and 100 μM of Gos, the residual activity was found to be ~ 22% and ~ 11%, respectively, and the IC_{50} of this molecule was 21.5 μM (Fig. 8A). In the second condition (ii), with 50 and 100 μM of Gos, the residual activity was found to be ~ 30% and ~ 13%, respectively, and the IC_{50} was approximately 23 μM (Fig. 8C). Importantly, CSB resulted to be the most effective inhibitor. In the first condition (i), a residual activity of the enzyme of about 14% was observed with 5 μM of CSB and was completely blocked with 50 μM CSB with an IC_{50} of 1.2 μM (Fig. 8B). In the second condition (ii), the residual activity was found to be ~ 30% and 0%, respectively, with 5 and 50 μM of CSB with an IC_{50} of approximately 1.5 μM. (Fig. 8D). Finally, flunixin meglumine appeared to be the least effective inhibitor since the residual activity of the enzyme with 100 μM of the compound was about 83% (data not shown).

The effect of the inhibitor CSB was then tested on the initial rate of FAD formation by extracts from PANC-1-derived CSCs. A concentration of 2 μM CSB had negligible inhibition of the initial rate of FAD synthesis, while 10 μM of the compound produced an 80% inhibition (Fig. 9). Consequently, an IC_{50} in this μM range is expected. For a more precise evaluation of this

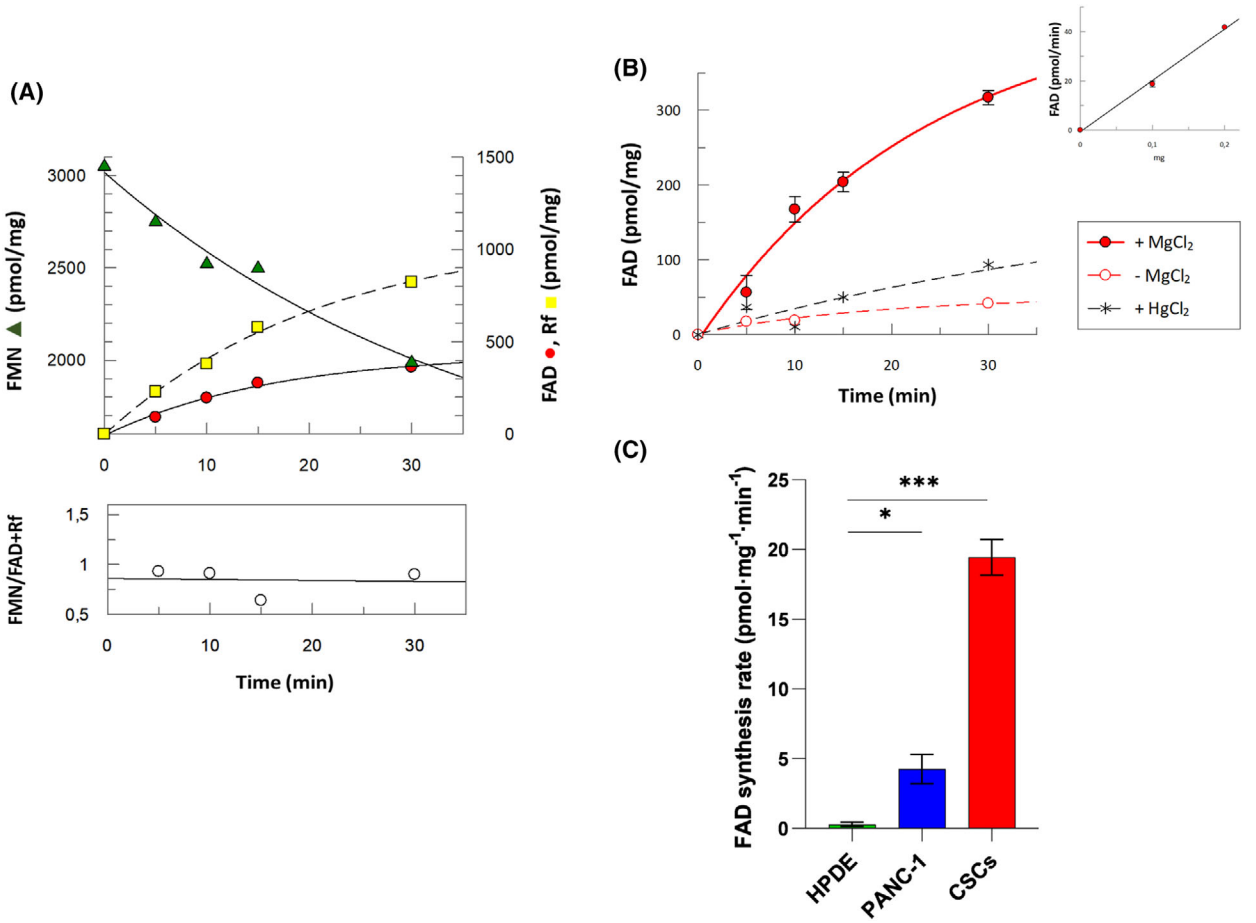

Fig. 6. FAD synthesis rate in HPDE, PANC-1 and PANC-1-derived CSCs. (A) Time course of FAD synthesis rate in PANC-1-derived CSCs. Experiments were performed at 37 °C in 50 mM Tris-Cl pH 7.5, with 5 mM $MgCl_2$, 1 μM FMN and 5 mM ATP in the presence of 100 μg of lysate. At the bottom is the ratio between the amount of FMN disappearance and the amount of FAD plus Rf measured in the cell lysates. (B) Time course of FAD synthesis rate in PANC-1-derived CSCs. Experiments were performed at 37 °C in 50 mM Tris-Cl pH 7.5, with 1 μM FMN, 5 mM ATP in the absence of 5 mM $MgCl_2$ (open circle) and in the presence of 5 mM $MgCl_2$ (closed circle) or in the presence of 5 mM $MgCl_2$ plus 5 μM $HgCl_2$ (asterisk). In the inset, dependence of FAD synthesis rate on mg of protein. (C) Histogram of FAD synthesis rate in HPDE, PANC-1 and PANC-1-derived CSCs. All data represent the results of three different experiments (mean ± SEM). Student's t-test: *$p \leq 0.05$ and *** $p \leq 0.001$.

number, further experimental efforts are necessary, especially to improve kinetics. The assay was also conducted in the presence of $HgCl_2$ and a residual activity of 60% was observed, in line with previous results [13].

PAPS domain of hFADS2 accommodates CSB

To investigate how FADS interacts with this compound, we performed a computational blind docking with the whole protein, from which two clusters of poses were detected for the FADSy domain. Thus, the docking analysis was restricted to the FADSy domain since it is responsible for the FAD synthesis. Interestingly, the CSB compound was docked in close contact with both the Flavin motif and PP loop, which have been demonstrated to be crucial for isoalloxazine ring and pyrophosphate binding respectively (Fig. 10) [12,40]. The Ki, that is, the half-saturation constant of the enzyme–inhibitor complex, calculated from the computational analysis by applying the equation: $Ki = \exp(\Delta G/(R \cdot T))$, for the pose with the highest score (lowest energy) was about 3.3×10^{-7} M, consistent with the IC_{50} value obtained experimentally with the purified protein.

CSB is more effective at inhibiting PANC-1-derived CSCs viability than either HPDE or PANC-1

To evaluate the effect of CSB on cell growth, we treated HPDE, PANC-1 and PANC-1-derived CSCs with

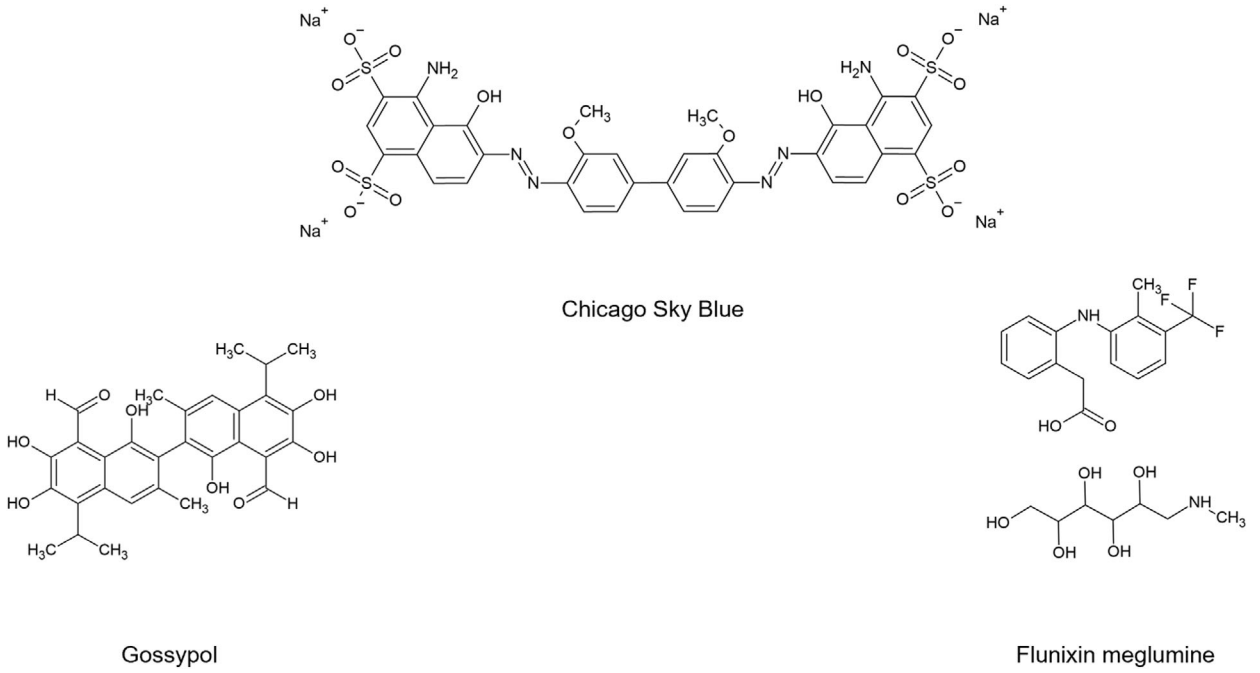

Fig. 7. Chemical structures of compounds selected as potential 6-His hFADS2 inhibitors. Potential inhibitors were selected among those published in [39]. Chemical structures were designed with ACD/ChemSketch for Academic and Personal Use: ACD/Labs.com, 2015.

increasing concentrations of CSB (5, 10, 25, 50, 100 and 200 μM) for 24, 48 and 72 h and cell viability was measured by using the Resazurin assay. As shown in Fig. 11, all cell lines responded to the drug in a dose-dependent manner over time but displayed a different growth sensitivity to CSB treatment. The HPDE were the less sensitive cells. The largest difference in sensitivity towards the inhibitor among HPDE and the other cell lines was observed at the lowest time of incubation, that is, 24 h. At this time, HPDE cell viability was unaffected by CSB at concentrations up to 25 μM; about 50% inhibition was observed only at 100 μM CSB (Fig. 11A). PANC-1 or PANC-1-derived CSCs were much more sensitive to the inhibitor at 24 h with about 50% inhibition at 50 μM (Fig. 11B) or 10 μM CSB (Fig. 11C) respectively. At longer times, that is, after 48 or 72 h, the difference in sensitivity to CSB was weakened, being the PANC-1-derived CSCs still the most sensitive at all times. The differences observed might be interpreted in terms of FAD synthase expression at basal levels in 'normal' HPDE cells. In this context, the inhibition by CSB may not be relevant for the overall process of cell growth. Higher concentrations (above 100 μM) or higher incubation times could inhibit molecular processes other than FAD synthesis, resulting in cell toxicity.

Interestingly, PANC-1-derived CSCs, the most sensitive to CSB, are known to be responsible for chemoresistance and tumour relapse, thus opening the possibility of application of CSB to more invasive tumour types.

Discussion

The goal of our present efforts was to understand whether and how FAD cofactor synthesis and delivery to apo-flavoproteins are important events during PDAC cells' malignant progression. Our models are PDAC cell lines transformed with two different mutated forms of the p53 protein, whose role in controlling and adapting tumour cell metabolism has been supported by a growing amount of evidence [41]. Quite importantly, co-authors of this paper have developed and characterized stem cells derived from PDAC cells [26,27], which are expected to be enriched in mitochondria compared to differentiated cells [2] and, therefore, offer the opportunity to gain further insight into the role of energy-linked flavoenzymes in transformation and stemness.

Another advantage of investigating CSCs' metabolism is the opportunity to search for more effective potential therapeutic drugs that are able to hit cancerous cell proliferation at a non-differentiated stage.

Keeping in mind the concept that FADS (EC2.7.7.2) is the product of a unique essential gene, that is, *FLAD1*, and that the process of forming FAD

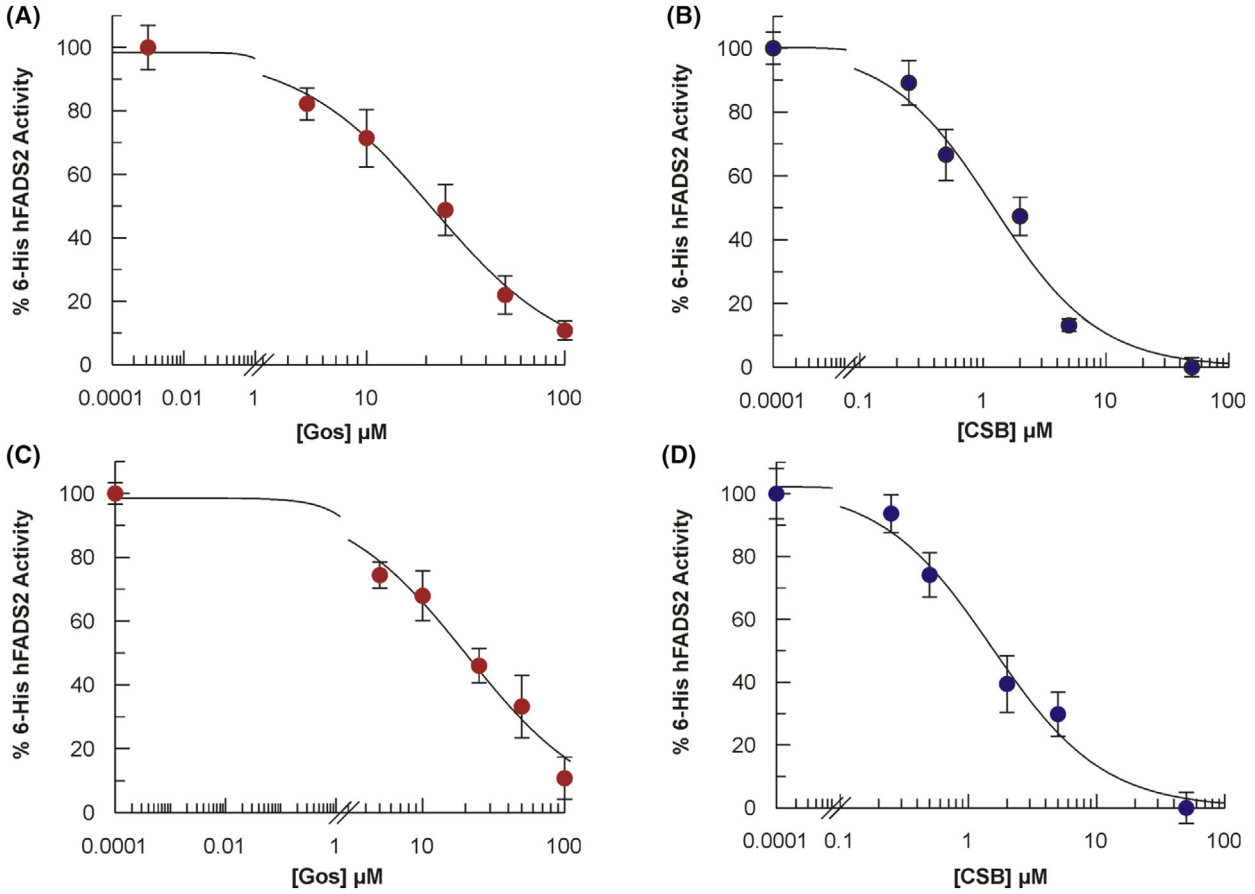

Fig. 8. Dose–response curve for the 6-His hFADS2 activity in the presence of increasing concentrations of Gos and CSB. (A, B) Experiments were performed at 37 °C in Tris-Cl 50 mM pH 7.5 with FMN 0.3 μM, ATP 25 μM and $MgCl_2$ 5 mM. (C, D) Experiments were performed at 37 °C in Tris-Cl 50 mM pH 7.5 with FMN 2 μM, ATP 100 μM and $MgCl_2$ 5 mM. All data represent the results of two different experiments (mean ± SEM).

is essential for cell bioenergetics, growth and regulation, we first addressed FADS in PANC-1 cells and their derived CSCs as a potentially overexpressed protein of the whole pathway of FAD formation (Fig. 1A). We got clear evidence that the cytosolic isoform of FADS, migrating on SDS/PAGE at about 54 kDa, is expressed at a greater level in PDAC cell lines and even more in CSCs, compared to HPDE, an immortalized cell line, expressing wt-p53 (Figs 1A and 3). In line with data obtained from the cBioPortal (Fig. 5), a similar increase was confirmed at the transcriptional level (Fig. 1B).

As shown in Fig. 6C, the overexpressed protein is fully enzymatically active. Therefore, we hypothesized that increased FAD synthesis responds to a higher demand for flavin cofactors to satisfy the increased expression of a flavoenzyme relevant for tumour epigenetics, such as the nuclear-located LSD1, whose overexpression was demonstrated (Fig. 2C,D). An increased FAD availability could also be necessary to follow the metabolic adaptive changes in SDHA, which are expected to parallel the cellular metabolic reprogramming from glycolytic towards oxidative when stemness is induced. The finding that an increase in SDHA protein is accompanied by an increase in its fluorescence (i.e. flavinylation, Fig. 2A, inset) provides further proof that the machinery that delivers FAD to nascent apo-flavoproteins [38] is working properly in these cells.

A point that requires further investigation in the frame of FAD delivery to apo-flavoproteins [8,38] concerns the subcellular localization of the overexpressed FADS, which in non-cancerous cells is expected to be localized principally in the cytosol. A different isoform, with a molecular mass of about 60 kDa [9], would be expected to ensure the biogenesis of mitochondrial flavoenzymes. A clear response to this biochemical problem and a direct assessment of the presence/absence of a mitochondrial isoform of FADS in these cell lines require selective PCR investigation,

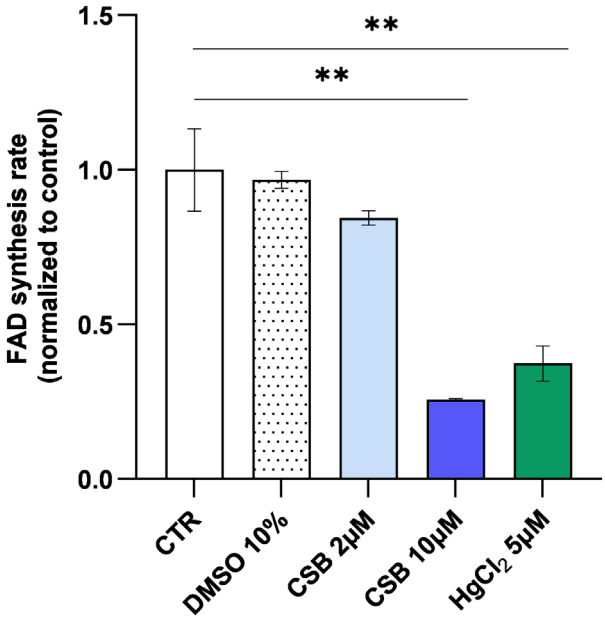

Fig. 9. FAD synthesis rate in PANC-1-derived CSCs in the presence of CSB. Experiments were performed at 37 °C in 50 mM Tris-Cl pH 7.5, with 5 mM $MgCl_2$, 0.5 μM FMN, 5 mM ATP, 5 μM $HgCl_2$, 10% dimethyl sulfoxide (DMSO) and 2 and 10 μM of CSB in the presence of 100 μg of lysate. All data represent the results of two different experiments (mean ± SEM). Ordinary one-way ANOVA: $^{**}p \leq 0.01$.

confocal microscopy and fractionation studies, such as those made in the past [7–9] and are currently ongoing in our laboratories. Nevertheless, supplier of FAD for this mitochondrial FADS isoform in malignant cells might reasonably be the SLC25A32 transporter, which was recently discovered to sustain cancer cell proliferation by regulating FAD metabolism in MiaPaCa2 cells [42]. Another point that might be interesting to deal with is some possible differences in FADS and/or SLC25A32 expression in female-derived pancreatic cancer cell lines. Indeed, even though we do not expect great variations on the basis of previous findings [43], we will further investigate this issue to get possible indications for tuning treatments in the frame of precision medicine.

The finding of a significant up-regulation of the FAD-forming enzymes in the CSCs, together with the development of an appropriate enzymatic assay to test potential inhibitors, such as CSB, allowed us to search for novel potential anticancer drugs. The effectiveness of CSB, which performs FADS-based antibiotic activity [39], was demonstrated by quite low levels of IC_{50} as measured on recombinant purified human protein [38] and which was also confirmed in PDAC cell total lysates. More importantly, the high potential of CSB as an anticancer drug was definitively demonstrated by its ability to inhibit cell growth of the PANC-1-derived CSCs (Fig. 11C). This compound was previously proposed as an agent capable of potentiating chemo- and radiotherapy treatments for cancer [44].

Based on its molecular complexity and the presence of a negative charge at physiological pH, this compound could enter the cells through organic anion transporters, which are known to be involved in the transport of other fluorescent dyes [45,46]. Indeed, the cell-line-specific inhibition of cell growth points towards the capability of this compound to enter the cells and reach the molecular target, as was already proposed for macrophages [25]. A precise assessment of the possible side effects on the neurological system is needed since it is known to inhibit glutamate uptake [47].

Similar growth-inhibiting properties were reported for FAD encapsulated in nanoparticles on MiaPaCa2 cell growth [48] and we speculate that this is due to the product inhibition of FADS [49,50]. Thus, the next step in our investigation could be to study the effects of a potential nano-delivery of the CSB on FADS

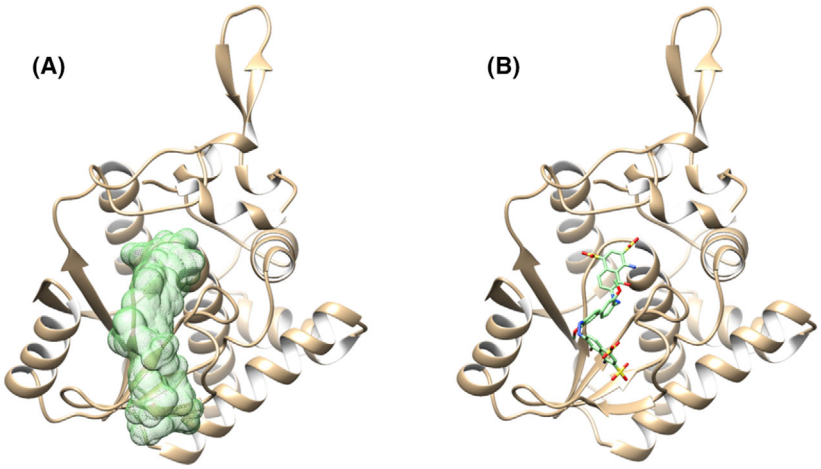

Fig. 10. Interaction of the CSB to hFADS2. The FADSy domain of hFADS2 protein derived from AlphaFold (retrieved 2022/06/16) is depicted in ribbon representation. (A) The cluster of poses obtained by blind docking is highlighted as green molecular surface. (B) The pose with the highest score, that is, low free energy (−8.8 Kcal·mol^{-1}) is depicted in licorice.

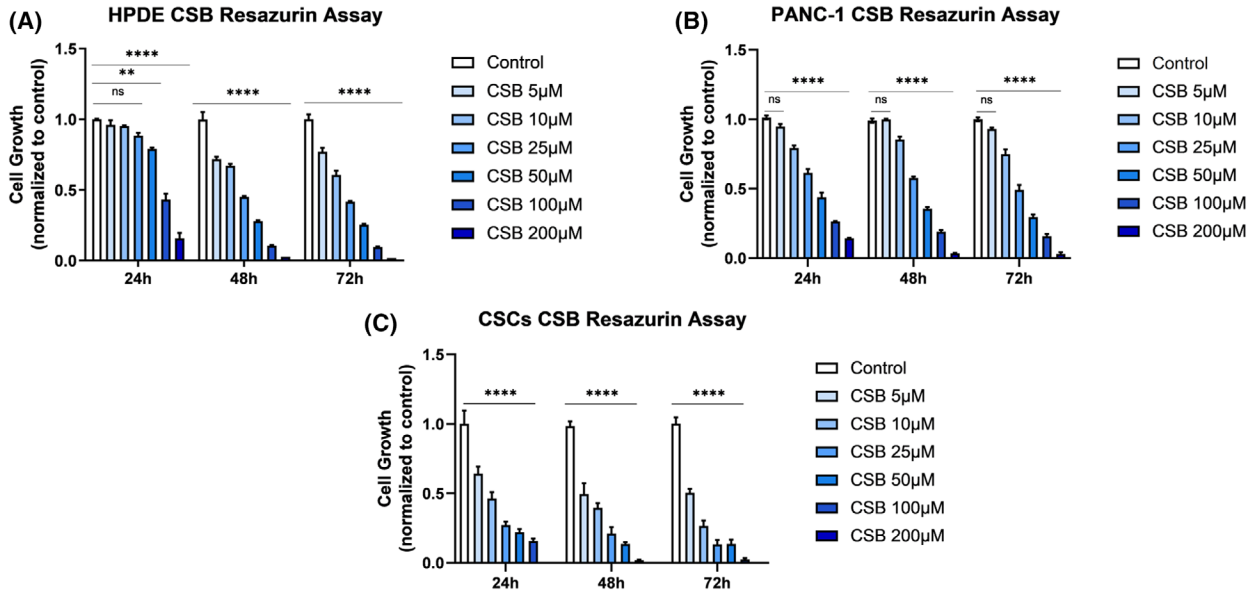

Fig. 11. Cell growth in the presence of CSB in HPDE, PANC-1 and PANC-1-derived CSCs. All experiments were conducted in (A) HPDE, (B) PANC-1 and (C) PANC-1-derived CSCs in the absence or presence of increasing CSB concentrations up to 72 h. Growth was measured using the Resazurin cell viability assay. Data are shown as mean ± SEM of two or three independent experiments performed in triplicate. Ordinary one-way ANOVA: ns $p > 0.05$; ** $p \leq 0.01$ and **** $p \leq 0.0001$.

activity and cell growth in the hope of further increasing its therapeutic potential.

Materials and methods

Cell cultures

PANC-1 and MiaPaCa2 cells were grown in RPMI 1640 supplemented with 10% FBS (fetal bovine serum), 2 mM glutamine and 50 $\mu g \cdot mL^{-1}$ gentamicin sulfate (Thermo Fisher Scientific, Waltham, MA, USA) and were kept at 37 °C in humidified air containing 5% CO_2. PANC-1- and MiaPaCa2-derived CSCs were generated as described in [26,27] and grown in DMEM/F-12 (Life Sciences) supplemented with 1 $g \cdot L^{-1}$ glucose, B27 (Thermo Fisher Scientific), 1 $\mu g \cdot mL^{-1}$ Fungizone (Thermo Fisher Scientific), 1% penicillin/streptomycin (Thermo Fisher Scientific), 5 $\mu g \cdot mL^{-1}$ heparin (Sigma-Aldrich), 20 $ng \cdot mL^{-1}$ EGF (Epidermal Growth Factor, Peprotech) and 20 $ng \cdot mL^{-1}$ FGF (Fibroblast Growth Factor, Peprotech) at 37 °C with 5% CO_2. HPDE cells were cultured in keratinocyte serum-free (KSF) media (Thermo Fisher Scientific) containing 1.6 $g \cdot L^{-1}$ glucose supplemented with EGF (5 $ng \cdot mL^{-1}$), bovine pituitary extract (BPE, 50 $\mu g \cdot mL^{-1}$) and penicillin–streptomycin.

Cell viability

Cell viability was measured using the Resazurin cell viability assay (Immunological Sciences, Rome, Italy) according to the manufacturer's instructions. The Resazurin method is an easy and fast assay to measure cell viability based on the principles of the MTT assay, with the superiority of not having to extract the dye from the cells. Cells (25×10^3 for both the PANC-1 and the CSCs and 4×10^4 for the HPDE) were seeded in 96-well plates and treated with different concentrations of CSB for 24, 48 and 72 h. After treatments, resazurin (15 μL) was added in 150 μL medium of each well, and fluorescence was measured after ~ 3 h of cell incubation at 37 °C by using a Varian Cary Eclipse Fluorescence Spectrophotometer (Agilent Technologies, Santa Clara, CA, EUA) at Ex/Em wavelengths of 535/590 nm [51]. The data obtained for each treatment were normalized with those obtained from their respective control group. All experiments were performed at least three times in triplicate.

Semi-quantitative and quantitative RT-PCR

Total cellular RNA was extracted from cells by using the RNeasy® Mini Kit (Qiagen, Cat# 74104) and reverse-transcribed to cDNA by using the RevertAid First Strand cDNA Synthesis Kit (Thermo Fisher Scientific, Cat# K1621) following the instructions of the manufacturer's protocols, essentially as in [52]. PCR was performed using Wonder-Taq – Taq polymerase (Euroclone, Pero (MI), Italy, Cat# EME020001) according to the manufacturer's instructions using gene-specific primers (*FLAD1* FW 5′–GCAGGTGCCCTACAGACCATT–3′ REV 5′–GTCTTTGCCCCCGTTGAAG–3′; *SDHA* FW 5′–GCATTATAACATGGGCGGC–3′ REV 5′–GCCTGCATGACTCTT

CGATG–3′; *β-actin* FW 5′–CTGGGAGTGGGT GGAGGC–3′ REV 5′–TCAACTGGTCTCAAGTCAGTG –3′, *LSD1* 5′–TTCAGGAGTTGGAAGCGAAT–3′ REV 5′–GAACCTGTCGCACTGCGTA–3′). RT-PCR products were separated by electrophoresis on a 2% agarose gel. Gene expression levels were analysed through a semiquantitative RT-PCR technique, using β-actin for expression-level normalization of the target genes. Images and quantification were obtained using the Image Lab™ software (Bio-Rad, Hercules, California, US, RRID:SCR_014210) of ChemiDoc™ (Bio-Rad) imaging system. Quantitative real-time PCR analysis was carried out using SYBR® Green PCR Master Mix (Applied biosystems, Cat# 4309155) according to the manufacturer's instructions using the gene-specific primers listed above.

Protein extraction and western blotting analysis

Total proteins from cell lines were extracted using a home-made lysis buffer containing 50 mM Tris/HCl (pH 7.5), 1% Triton X-100, 5 mM β-mercaptoethanol, 1 mM NaF, 0.1 mM phenylmethylsulfonyl fluoride (PMSF) and 1× protease-inhibitor cocktail, and the resulting cell suspension passed first through a 22G needle and then a 26G needle. The cell suspension was centrifuged at 13 000 ***g*** for 10 min at 4 °C after incubation for 30 min on ice, and the supernatant was recovered as cell lysate. The protein concentration is quantified by a standard Bradford assay (Bio-Rad Laboratories), equal amounts of protein (0.05 mg) were separated by SDS/PAGE and then transferred onto a polyvinylidene difluoride membrane (Amersham™ Hybond™, Cat# 10600023). The primary antibodies were directed against the following proteins: FADS (International Application number PCT/IT2009/000062 filed on 23 February 2009, by Barile, Torchetti, Indiveri, Galluccio), SDHA (Molecular probes, 1 : 2000 dilution, Cat# A11142, RRID:AB_221579), α-tubulin (Sigma-Aldrich, 1 : 5000 dilution, Cat# T5168, RRID:AB_477579), LSD1 (Santa Cruz Biotechnology, Dallas, Texas, US, 1 : 1000 dilution, Cat# sc-271 720, RRID:AB_10709306) and glyceraldehyde-3-phosphate dehydrogenase (GAPDH) (Cell Signalling, 1 : 10 000 dilution, Cat# 2118, RRID: AB_561053). The bound antibodies were visualized with the aid of secondary anti-rabbit or anti-mouse IgG antibodies conjugated with peroxidase (1 : 2500 dilution). ECL western blotting detection reagents (GE Healthcare, Amersham, UK, Cat# RPN2209) were used for protein detection according to the manufacturer's recommendations. Densitometry was performed using the Image Lab™ software (Bio-Rad, RRID: SCR_014210) of ChemiDoc™ (Bio-Rad) imaging system.

UV fluorescence analysis

Proteins from cell lysates (0.04 mg) were separated by SDS/PAGE, then the unstained gel was incubated for 1 h in 10% acetic acid and inspected on an UV-transilluminator system. Upon illumination with UV light, the flavinylated flavoprotein subunit of SDH (SDHA) was visible because of the fluorescence of the covalently bound flavin. Protein bands on the gel were then stained with Coomassie Blue. Quantitative evaluations were carried out using the Image Lab™ software (Bio-Rad, RRID:SCR_014210) of ChemiDoc™ (Bio-Rad) imaging system.

Measurement of FAD synthesis rate in cell lysates

Cell lysates were obtained, and the protein amount was measured as described above. The FAD synthesis rate was measured essentially as in [53]. In summary, the assay was carried out at 37 °C in 600 μL of 50 mM Tris–HCl (pH 7.5) in the presence of 0.1 mg cell lysate, 1 μM flavin mononucleotide (FMN), 5 mM ATP and 5 mM $MgCl_2$. At different time points, 100 μL aliquots were extracted with perchloric acid and neutralized. Quantitative determination of Rf, FMN and FAD was carried out with a calibration curve made in each experiment with standard solutions diluted in the extraction solution. The amount of FAD formed (ΔFAD) is calculated by subtracting the endogenous FAD amount (reaction time 0 min) from the amount of FAD calculated at each time. The rate of FAD formation is calculated by plotting ΔFAD (pmol·mg^{-1}·protein^{-1}) versus time as in the typical discontinuous plot curve. The initial rate v_0 corresponds to the slope of the experimental line and it is expressed as pmol·mg protein^{-1}·min^{-1}. If the reaction rate is high (the curve reaches a plateau), the values of ΔFAD (pmol·mg protein^{-1}) as a function of time can be fitted with GraFit 5 program (or equivalent) to first-order rate equation. The initial rate v_0 is calculated by multiplying the limit value by the rate constant value [36].

Purification of recombinant 6-His hFADS2 and measurements of FAD synthesis rate

6His-hFADS2 purification was performed by immobilized metal chelate affinity chromatography (IMAC) starting from the soluble-cell fraction obtained from Rosetta (DE3) pLysS strain, transformed with WT hFADS2 cDNA cloned in pH6EX3 plasmid as previously described [38]. Fractions containing the purified recombinant protein were desalted on a PD10 column run in 40 mM Hepes/Na and 5 mM 2-ME, pH 7.4. The rate of FAD synthesis was measured as in [38] by exploiting the different fluorescence properties of FAD with respect to FMN. Fluorescence time courses (λ excitation at 450 nm; λ emission at 520 nm) were followed at 37 °C in a FP-3800 spectrofluorometer (Jasco, Easton, MD, USA). In each experiment, FAD and FMN fluorescence were calibrated by using standard solutions. The rate of FAD synthesis, expressed as nmol FAD·min^{-1}·(mg·protein)$^{-1}$, was calculated from the rate of fluorescence decrease, measured as the tangent to the initial part of the

experimental curve, as described in detail in [38]. For activity measurements, purified protein fractions (5–10 μg, 0.13–0.26 nmol protein as monomer, unless otherwise indicated) were incubated at 37 °C in 50 mM Tris/HCl, pH 7.5, containing 5 mM $MgCl_2$, 0.3 μM FMN, 25 μM ATP and additional reagents as appropriate. For inhibition analysis, the same conditions were used, except for substrates concentration (0.3 μM FMN and 25 μM ATP, 2 μM FMN and 100 μM ATP).

Chemicals

Chemicals were selected based on [39] and were from Sigma Aldrich (Gossypol, Cat# G4382; Chicago Sky Blue, Cat# C8679; Flunixin Meglumine, Cat# F0429).

Docking of CSB to the PAPS domain of hFADS2

The PDB file for the FADS was downloaded from the AlphaFold protein structure database (https://alphafold.ebi.ac.uk/entry/Q8NFF5). The canonical SMILES of the structure of CSB was retrieved from PubChem Database (https://pubchem.ncbi.nlm.nih.gov/#) and saved as .mol2 by ACD/ChemSketch software after removing sodium ions. The ligand and the protein were prepared using AUTO DOCK TOOLS (ADT) [54]. Gasteiger charge was assigned, and the files were saved in PDBQT format. Blind molecular docking was performed by AUTODOCK VINA v.1.1.2 [55]. The grid size covering the whole protein was set to 78 × 64 × 72 Å (x, y and z) with spacing 1. Two clusters of poses close to the FADSy domain were detected. The docking analysis was repeated eight times, restricting the protein to the sole FADSy domain. The resulting 72 poses were inspected using Chimera 1.16 [56].

Statistical analysis

Data were assessed for statistical significance using the Student's t-test and Ordinary One-Way ANOVA, performed using GRAPHPAD PRISM version 9.0.0 for Windows, GraphPad Prism Software, San Diego, CA, USA, www.graphpad.com (RRID:SCR_002798). Data are expressed as means ± SEM with n equal to the number of experiments. $p < 0.05$ was considered statistically significant.

Acknowledgements

This work could not have been conceived and carried out without the scientific and vital energy of the late Prof Massimo Tommasino, a wonderful youth friend of most of the authors. Whoever had the fortune to meet him has been invested in his excellence in science, cordiality and love. In the last period, his mission was to come back home to Apulia, Italy, and to co-opt young scientists from this region to fight cancer through research. All the authors will remember him forever. The helpful collaboration of Dr Teresa Anna Giancaspero and student Mariasandra Squicciarino, who participated in the early stages of this work, is also gratefully acknowledged. This work was supported by a grant from Association d'Aide a la Recherche sur les Therapies Innovative "Role of flavins in therapy" (2018–20) to MB, MCIN/AEI/10.13039/501100011033 (Grant number PID2019-103901GB-I00) to MM and by University of Calabria, progetti "ex 60% – The nutrient traffic in cells: link with human pathologies" 2021 to CI and the Marie Skłodowska-Curie grant agreement No. 813834–pHioniC–H2020-MSCA-ITN-2018 to SJR and RAC.

Conflict of interest

The authors declare no conflict of interest.

Author contributions

Conceptualization: AN and MB; Methodology: SJR and RAC; Formal analysis and investigation: AN, TMAC, DDM, MT, PL and MG; Writing – original draft preparation: AN and MB; Writing – review and editing: AN, MM, CI, SJR and RAC; Funding acquisition: MM, CI and MB; and Supervision: MB.

Data availability statement

The datasets analysed in this study are available in the cBioPortal for Cancer Genomics database at https://www.cbioportal.org/results/cancerTypesSummary; https://www.cbioportal.org/results/FLAD1survival.

References

1 Lambert A, Conroy T & Ducreux M (2021) Future directions in drug development in pancreatic cancer. *Semin Oncol* **48**, 47–56.
2 Tanabe A & Sahara H (2020) The metabolic heterogeneity and flexibility of cancer stem cells. *Cancer* **12**, 2780.
3 Feng Z, Shi M, Li K, Ma Y, Jiang L, Chen H & Peng C (2020) Development and validation of a cancer stem cell-related signature for prognostic prediction in pancreatic ductal adenocarcinoma. *J Transl Med* **18**, 360.
4 Leone A, Roca MS, Ciardiello C, Costantini S & Budillon A (2017) Oxidative stress gene expression profile correlates with cancer patient poor prognosis: identification of crucial pathways might select novel

therapeutic approaches. *Oxid Med Cell Longev* **2017**, 2597581.
5 Barile M, Giancaspero TA, Leone P, Galluccio M & Indiveri C (2016) Riboflavin transport and metabolism in humans. *J Inherit Metab Dis* **39**, 545–557.
6 Olsen RKJ, Konarikova E, Giancaspero TA, Mosegaard S, Boczonadi V, Matakovic L, Veauville-Merllie A, Terrile C, Schwarzmayr T, Haack TB *et al.* (2016) Riboflavin-responsive and -non-responsive mutations in FAD synthase cause multiple acyl-CoA dehydrogenase and combined respiratory-chain deficiency. *Am J Hum Genet* **98**, 1130–1145.
7 Giancaspero TA, Busco G, Panebianco C, Carmone C, Miccolis A, Liuzzi GM, Colella M & Barile M (2013) FAD synthesis and degradation in the nucleus create a local flavin cofactor pool. *J Biol Chem* **288**, 29069–29080.
8 Giancaspero TA, Colella M, Brizio C, Difonzo G, Fiorino GM, Leone P, Brandsch R, Bonomi F, Iametti S & Barile M (2015) Remaining challenges in cellular flavin cofactor homeostasis and flavoprotein biogenesis. *Front Chem* **3**, 30.
9 Torchetti EM, Brizio C, Colella M, Galluccio M, Giancaspero TA, Indiveri C, Roberti M & Barile M (2010) Mitochondrial localization of human FAD synthetase isoform 1. *Mitochondrion* **10**, 263–273.
10 Brizio C, Galluccio M, Wait R, Torchetti EM, Bafunno V, Accardi R, Gianazza E, Indiveri C & Barile M (2006) Over-expression in Escherichia coli and characterization of two recombinant isoforms of human FAD synthetase. *Biochem Biophys Res Commun* **344**, 1008–1016.
11 Leone P, Galluccio M, Brizio C, Barbiroli A, Iametti S, Indiveri C & Barile M (2019) The hidden side of the human FAD synthase 2. *Int J Biol Macromol* **138**, 986–995.
12 Miccolis A, Galluccio M, Giancaspero TA, Indiveri C & Barile M (2012) Bacterial over-expression and purification of the 3'phosphoadenosine 5'phosphosulfate (PAPS) reductase domain of human FAD synthase: functional characterization and homology modeling. *Int J Mol Sci* **13**, 16880–16898.
13 Leone P, Galluccio M, Barbiroli A, Eberini I, Tolomeo M, Vrenna F, Gianazza E, Iametti S, Bonomi F, Indiveri C *et al.* (2018) Bacterial production, characterization and protein modeling of a novel monofuctional isoform of FAD synthase in humans: an emergency protein? *Molecules* **23**, 116.
14 Powers HJ (2003) Riboflavin (vitamin B-2) and health. *Am J Clin Nutr* **77**, 1352–1360.
15 Eli M, Li DS, Zhang WW, Kong B, Du CS, Wumar M, Mamtimin B, Sheyhidin I & Hasim A (2012) Decreased blood riboflavin levels are correlated with defective expression of RFT2 gene in gastric cancer. *World J Gastroenterol* **18**, 3112–3118.
16 Fu T, Liu Y, Wang Q, Sun Z, Di H, Fan W, Liu M & Wang J (2016) Overexpression of riboflavin transporter 2 contributes toward progression and invasion of glioma. *Neuroreport* **27**, 1167–1173.
17 Long L, Pang XX, Lei F, Zhang JS, Wang W, Liao LD, Xu XE, He JZ, Wu JY, Wu ZY *et al.* (2018) SLC52A3 expression is activated by NF-kappaB p65/Rel-B and serves as a prognostic biomarker in esophageal cancer. *Cell Mol Life Sci* **75**, 2643–2661.
18 Aili A, Hasim A, Kelimu A, Guo X, Mamtimin B, Abudula A & Upur H (2013) Association of the plasma and tissue riboflavin levels with C20orf54 expression in cervical lesions and its relationship to HPV16 infection. *PLoS One* **8**, e79937.
19 Bartmann L, Schumacher D, von Stillfried S, Sternkopf M, Alampour-Rajabi S, van Zandvoort M, Kiessling F & Wu Z (2019) Evaluation of riboflavin transporters as targets for drug delivery and Theranostics. *Front Pharmacol* **10**, 79.
20 Tutino V, Defrancesco ML, Tolomeo M, De Nunzio V, Lorusso D, Paleni D, Caruso MG, Notarnicola M & Barile M (2018) The expression of riboflavin transporters in human colorectal cancer. *Anticancer Res* **38**, 2659–2667.
21 Hu P, Pan Y, Wang C, Zhang W, Huang H, Wang J & Zhang N (2020) FLAD1 is up-regulated in gastric cancer and is a potential prediction of prognosis. *Int J Med Sci* **17**, 1763–1772.
22 Mei M, Song W, Wang Y & Zhang M (2021) Significant diagnostic and prognostic value of FLAD1 and related MicroRNAs in breast cancer after a Pan-cancer analysis. *Dis Markers* **2021**, 6962526.
23 Stein Y, Rotter V & Aloni-Grinstein R (2019) Gain-of-function mutant p53: all the roads Lead to tumorigenesis. *Int J Mol Sci* **20**, 6197.
24 Ouyang H, Mou L, Luk C, Liu N, Karaskova J, Squire J & Tsao MS (2000) Immortal human pancreatic duct epithelial cell lines with near normal genotype and phenotype. *Am J Pathol* **157**, 1623–1631.
25 Jin K, Zheng L, Ye L, Xie Z, Gao J, Lou C, Pan W, Pan B, Liu S, Chen Z *et al.* (2021) Chicago sky blue 6B (CSB6B), an allosteric inhibitor of macrophage migration inhibitory factor (MIF), suppresses osteoclastogenesis and promotes osteogenesis through the inhibition of the NF-kappaB signaling pathway. *Biochem Pharmacol* **192**, 114734.
26 Dalla Pozza E, Dando I, Biondani G, Brandi J, Costanzo C, Zoratti E, Fassan M, Boschi F, Melisi D, Cecconi D *et al.* (2015) Pancreatic ductal adenocarcinoma cell lines display a plastic ability to bi-directionally convert into cancer stem cells. *Int J Oncol* **46**, 1099–1108.
27 Biondani G, Zeeberg K, Greco MR, Cannone S, Dando I, Dalla Pozza E, Mastrodonato M, Forciniti S, Casavola V, Palmieri M *et al.* (2018) Extracellular

matrix composition modulates PDAC parenchymal and stem cell plasticity and behavior through the secretome. *FEBS J* **285**, 2104–2124.
28 Kim HJ & Winge DR (2013) Emerging concepts in the flavinylation of succinate dehydrogenase. *Biochim Biophys Acta* **1827**, 627–636.
29 Fabian A, Stegner S, Miarka L, Zimmermann J, Lenk L, Rahn S, Buttlar J, Viol F, Knaack H, Esser D *et al.* (2019) Metastasis of pancreatic cancer: an uninflamed liver micromilieu controls cell growth and cancer stem cell properties by oxidative phosphorylation in pancreatic ductal epithelial cells. *Cancer Lett* **453**, 95–106.
30 Brizio C, Brandsch R, Bufano D, Pochini L, Indiveri C & Barile M (2004) Over-expression in Escherichia coli, functional characterization and refolding of rat dimethylglycine dehydrogenase. *Protein Expr Purif* **37**, 434–442.
31 Giancaspero TA, Wait R, Boles E & Barile M (2008) Succinate dehydrogenase flavoprotein subunit expression in *Saccharomyces cerevisiae*–involvement of the mitochondrial FAD transporter, Flx1p. *FEBS J* **275**, 1103–1117.
32 Sharma P, Maklashina E, Cecchini G & Iverson TM (2020) The roles of SDHAF2 and dicarboxylate in covalent flavinylation of SDHA, the human complex II flavoprotein. *Proc Natl Acad Sci USA* **117**, 23548–23556.
33 Dong J, Pervaiz W, Tayyab B, Li D, Kang L, Zhang H, Gong H, Ma X, Li J, Agboyibor C *et al.* (2022) A comprehensive comparative study on LSD1 in different cancers and tumor specific LSD1 inhibitors. *Eur J Med Chem* **240**, 114564.
34 Hosseini A & Minucci S (2017) A comprehensive review of lysine-specific demethylase 1 and its roles in cancer. *Epigenomics* **9**, 1123–1142.
35 Hino S, Sakamoto A, Nagaoka K, Anan K, Wang Y, Mimasu S, Umehara T, Yokoyama S, Kosai K & Nakao M (2012) FAD-dependent lysine-specific demethylase-1 regulates cellular energy expenditure. *Nat Commun* **3**, 758.
36 Leone P, Tolomeo M & Barile M (2021) Continuous and discontinuous approaches to study FAD synthesis and degradation catalyzed by purified recombinant FAD synthase or cellular fractions. *Methods Mol Biol* **2280**, 87–116.
37 Barile M, Brizio C, De Virgilio C, Delfine S, Quagliariello E & Passarella S (1997) Flavin adenine dinucleotide and flavin mononucleotide metabolism in rat liver–the occurrence of FAD pyrophosphatase and FMN phosphohydrolase in isolated mitochondria. *Eur J Biochem* **249**, 777–785.
38 Torchetti EM, Bonomi F, Galluccio M, Gianazza E, Giancaspero TA, Iametti S, Indiveri C & Barile M (2011) Human FAD synthase (isoform 2): a component of the machinery that delivers FAD to apo-flavoproteins. *FEBS J* **278**, 4434–4449.
39 Sebastian M, Anoz-Carbonell E, Gracia B, Cossio P, Ainsa JA, Lans I & Medina M (2018) Discovery of antimicrobial compounds targeting bacterial type FAD synthetases. *J Enzyme Inhib Med Chem* **33**, 241–254.
40 Huerta C, Borek D, Machius M, Grishin NV & Zhang H (2009) Structure and mechanism of a eukaryotic FMN adenylyltransferase. *J Mol Biol* **389**, 388–400.
41 Mantovani F, Collavin L & Del Sal G (2019) Mutant p53 as a guardian of the cancer cell. *Cell Death Differ* **26**, 199–212.
42 Santoro V, Kovalenko I, Vriens K, Christen S, Bernthaler A, Haegebarth A, Fendt SM & Christian S (2020) SLC25A32 sustains cancer cell proliferation by regulating flavin adenine nucleotide (FAD) metabolism. *Oncotarget* **11**, 801–812.
43 Muscogiuri G, Barrea L, Feola T, Gallo M, Messina E, Venneri MA, Faggiano A & Colao A (2020) Pancreatic neuroendocrine neoplasms: does sex matter? *Trends Endocrinol Metab* **31**, 631–641.
44 Normand A, Riviere E & Renodon-Corniere A (2014) Identification and characterization of human Rad51 inhibitors by screening of an existing drug library. *Biochem Pharmacol* **91**, 293–300.
45 Bakos E, Tusnady GE, Nemet O, Patik I, Magyar C, Nemeth K, Kele P & Ozvegy-Laczka C (2020) Synergistic transport of a fluorescent coumarin probe marks coumarins as pharmacological modulators of organic anion-transporting polypeptide, OATP3A1. *Biochem Pharmacol* **182**, 114250.
46 Lipman BJ, Silverstein SC & Steinberg TH (1990) Organic anion transport in macrophage membrane vesicles. *J Biol Chem* **265**, 2142–2147.
47 He Z, Yan L, Yong Z, Dong Z, Dong H & Gong Z (2013) Chicago sky blue 6B, a vesicular glutamate transporters inhibitor, attenuates methamphetamine-induced hyperactivity and behavioral sensitization in mice. *Behav Brain Res* **239**, 172–176.
48 Arib C, Bouchemal N, Barile M, Paleni D, Djaker N, Dupont N & Spadavecchia J (2021) Flavin-adenine-dinucleotide gold complex nanoparticles: chemical modeling design, physico-chemical assessment and perspectives in nanomedicine. *Nanoscale Adv* **3**, 6144–6156.
49 Huerta C, Grishin NV & Zhang H (2013) The "super mutant" of yeast FMN adenylyltransferase enhances the enzyme turnover rate by attenuating product inhibition. *Biochemistry* **52**, 3615–3617.
50 Leone P, Galluccio M, Quarta S, Anoz-Carbonell E, Medina M, Indiveri C & Barile M (2019) Mutation of aspartate 238 in FAD synthase isoform 6 increases the specific activity by weakening the FAD binding. *Int J Mol Sci* **20**, 6203.

51 Zeeberg K, Cardone RA, Greco MR, Saccomano M, Nohr-Nielsen A, Alves F, Pedersen SF & Reshkin SJ (2016) Assessment of different 3D culture systems to study tumor phenotype and chemosensitivity in pancreatic ductal adenocarcinoma. *Int J Oncol* **49**, 243–252.

52 Tolomeo M, Chimienti G, Lanza M, Barbaro R, Nisco A, Latronico T, Leone P, Petrosillo G, Liuzzi GM, Ryder B *et al*. (2022) Retrograde response to mitochondrial dysfunctions associated to LOF variations in FLAD1 exon 2: unraveling the importance of RFVT2. *Free Radic Res* **56**, 511–525.

53 Ryder B, Tolomeo M, Nochi Z, Colella M, Barile M, Olsen RK & Inbar-Feigenberg M (2019) A novel truncating FLAD1 variant, causing multiple acyl-CoA dehydrogenase deficiency (MADD) in an 8-year-old boy. *JIMD Reports* **45**, 37–44.

54 Morris GM, Huey R, Lindstrom W, Sanner MF, Belew RK, Goodsell DS & Olson AJ (2009) AutoDock4 and AutoDockTools4: automated docking with selective receptor flexibility. *J Comput Chem* **30**, 2785–2791.

55 Trott O & Olson AJ (2010) AutoDock Vina: improving the speed and accuracy of docking with a new scoring function, efficient optimization, and multithreading. *J Comput Chem* **31**, 455–461.

56 Pettersen EF, Goddard TD, Huang CC, Couch GS, Greenblatt DM, Meng EC & Ferrin TE (2004) UCSF chimera–a visualization system for exploratory research and analysis. *J Comput Chem* **25**, 1605–1612.